High-Q TM whispering-gallery modes in three-dimensional microcylinders

Yue-De Yang, Yong-Zhen Huang, and Qin Chen
State Key Laboratory on Integrated Optoelectronics, Institute of Semiconductors, Chinese Academy of Sciences, P.O. Box 912, Beijing 100083, China
(Received 26 July 2006; published 30 January 2007)

We present a generation condition for realizing high-Q TM whispering-gallery modes (WGMs) in semiconductor microcylinders. For microcylinders with symmetry or weak asymmetry vertical waveguiding, we show that TM WGMs can have a high Q factor, with the magnitude of 10^4 at the radius of the microcylinder of 1 μm, by three-dimensional numerical simulation. The Q factor of TE WGMs is much less than that of TM WGMs in the semiconductor microcylinders due to a vertical radiation loss caused by mode coupling with the vertical propagating mode. The results open up a possible application of TM WGMs in semiconductor microcylinders for efficient current injection microlasers and single photon sources.

DOI: 10.1103/PhysRevA.75.013817 PACS number(s): 42.79.Gn, 42.79.Ci, 42.79.Vb, 85.60.−q

I. INTRODUCTION

High-Q optical microcavities have a lot of applications in physics and engineering, such as strong-coupling cavity quantum electrodynamics, enhancement, and suppression of spontaneous emission, novel sources, and dynamic filters in optical communication [1]. A strong enhancement of the spontaneous emission rate (Purcell effect) was observed for self-assembled InAs/GaAs quantum dots in micropillar cavities and microdisks [2], and a single photon source was expected by inserting an on resonance single quantum dot in a three-dimensional (3D) microcavity. A single-photon turnstile device was demonstrated in a microdisk with a quantum dot using pulsed laser excitation [3], and efficient production of triggered single photons was obtained by coupling a single semiconductor quantum dot to a 3D micropillar cavity, which was vertically confined by upper and below distributed-Bragg reflectors (DBRs) [4]. Furthermore, a two-dimensional (2D) photonic crystal nanocavity was realized with the Q factor of 4.5×10^4 and a very small modal volume of $V=7.0\times10^{-14}$ cm^3 [5], which will have strong Purcell effect due to the extremely large Q/V value.

Semiconductor microdisks with whispering-gallery modes (WGMs) can have low modal volume, high Q factor, and a large spontaneous emission factor [6,7]. In the ray picture, the light of WGMs is laterally trapped inside the cavity through total internal reflections on the cavity-air boundary, and vertically confined by a large refractive index difference. The Q factor of 4.7×10^5, which was practically limited by Rayleigh scattering from surface roughness, was measured for TM WGMs in a 344-nm-thickness silicon microdisk with the radius of 2.5 μm in the 1550 nm wavelength band [8]. Electrically pumped quantum-dot microcylinder laser was realized at room temperature [9], which was still based on TE polarization WGMs as in microdisk lasers [10]. The WGMs in semiconductor microcylinders are vertically confined by a slab waveguiding as that of a conventional edge-emitting semiconductor laser, so microcylinder resonators have better thermal conductivity and current injection efficiency than the microdisk on a pedal and the pillar microstructures with DBRs. For TE WGMs, Q factors of 10^4 and 10^{10} at wavelength about 1.5 μm were predicted by 3D finite-difference time-domain (FDTD) simulation for microdisks with the radius of 1 and 2 μm, respectively [11]. But the Q factors reduce to the order of 10^2 for TE WGMs in the semiconductor microcylinder at the radius of 1 μm, as the refractive indices of the center layer and cladding layers to be 3.4 and 3.

II. INFLUENCE OF THE PROPAGATING MODES

In this paper, we investigate mode characteristics and determine a general condition required to achieve high-Q WGMs in semiconductor microcylinders. In a microcylinder with a weak vertical waveguiding, the vertical radiation will play an important role in determining the Q factors of the WGMs. The transverse electric and transverse magnetic $TE_{m,l}$ and $TM_{m,l}$ WGMs in the microcylinder, where the vertical mode number is ignored and m and l are the azimuthal and radial mode numbers, will coupled with the vertical propagating $EH_{m,l}$ and $HE_{m,l}$ modes in the corresponding circular waveguide of the cladding layers. The cutoff wavelengths of the guided and radiated $EH_{m,l}$ and $HE_{m,l}$ modes can be obtained as their vertical propagation constant $\beta=0$, which are the same as the mode wavelengths of $TE_{m,l}$ and $TM_{m,l}$ WGMs in a 2D microdisk with the refractive index of the cladding layer, respectively. For a microcylinder with the radius $R=1$ μm, the center layer thickness $d=0.2$ μm, and the vertical refractive index distribution of $n_2/n_1=3.4/n_2$, the mode wavelengths of the $TE_{7,1}$ and $TM_{7,1}$ WGMs obtained from the 2D eigenvalue equations [12] under the effective index approximation are plotted as the dashed and solid lines in Fig. 1, respectively, and the cutoff wavelengths of the radiated $EH_{7,1}$ and $HE_{7,1}$ are plotted as dash-dotted and dotted lines. Two crossover points exist between $TE_{7,1}$ and $TM_{7,1}$ WGMs near $n_2=2.3$ and between $TE_{7,1}$ and $HE_{7,1}$ near $n_2=2.65$. We can expect that the mode coupling between $TE_{7,1}$ and $HE_{7,1}$ will result in a large vertical radiation loss as the mode wavelength of $TE_{7,1}$ is smaller than the cutoff wavelength of $HE_{7,1}$ mode. The mode wavelength of $TM_{7,1}$ is larger than that of $TE_{7,1}$ as $n_2>2.3$, and does not cross with those of the $HE_{7,1}$ and $EH_{7,1}$ modes. So the mode coupling with the vertically propagating modes does not exist for the TM WGMs, and the TM WGMs will have high Q

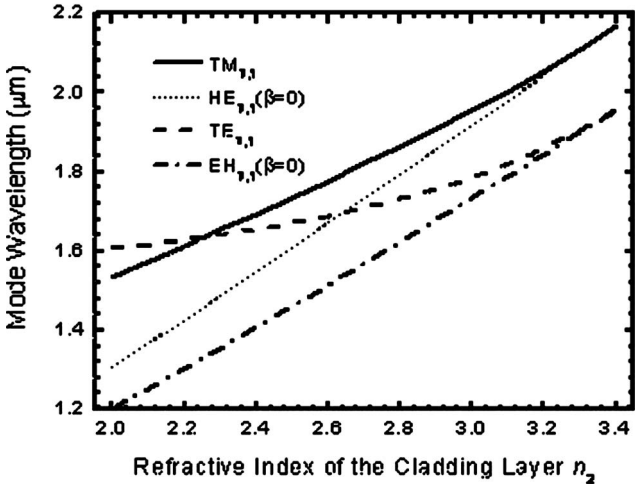

FIG. 1. Mode wavelengths of $TE_{7,1}$ and $TM_{7,1}$ WGMs obtained from 2D eigenvalue equation under the effective index approximation versus n_2 are plotted as solid and dashed lines, respectively, for the symmetrical microcylinder with radius $R=1$ μm, $d=0.2$ μm, and $n_1=3.4$. The cutoff wavelengths of the radiated $EH_{7,1}$ and $HE_{7,1}$ modes in the corresponding microwire with the refractive index n_2 are plotted as the dash-dotted and dotted lines.

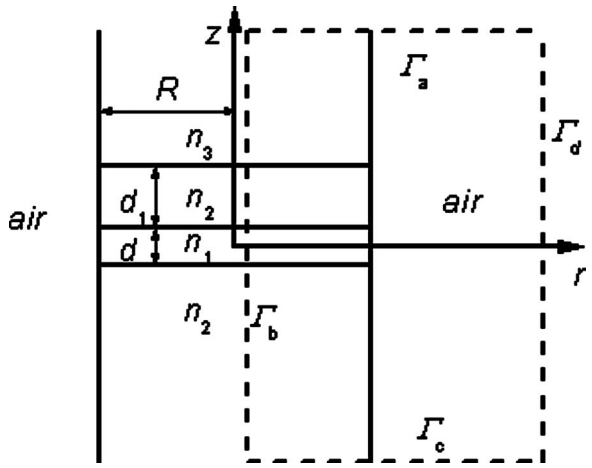

FIG. 2. Cross section of a microcylinder with the refractive index distribution $n(z)$ of $n_2/n_1/n_2/n_3$, and the thicknesses of center layer and upper cladding layer of d and d_1. The FDTD simulation region is bounded by Γ_a, Γ_b, Γ_c, and Γ_d.

factors. It should be noted that the above phenomena exist for the TE and TM WGMs with different mode numbers and are mainly affected by the refractive index difference n_1-n_2. For a microcylinder with $R=1$ μm, $d=0.2$ μm, and $n_1=3.5$, we have the crossover points at $n_2=2.45$ and 2.85 as the mode index $m=9$. In fact, the phenomena are universal in microcylinder resonators with weak waveguides, because the wavelengths of TE modes with effective refractive index n_{eff} usually smaller than those of TM modes with the refractive index of the cladding layer n_2 when the differences between refractive indices of the center layer and cladding layer and the sizes of the resonators are small.

III. NUMERICAL MODEL

To verify the above argument, we simulate the mode characteristics for microcylinders by 3D FDTD technique. The FDTD method was first introduced by Yee in 1966 for solving Maxwell's curl equations directly in the time domain on a space grid [13], and was rapidly developed and widely used in modeling optical microcavity [14]. Based on the circular symmetry, the 3D problem of a microcylinder can be transformed into a 2D one with the angular field dependence of $\exp(im\varphi)$ [15], where m is the azimuthal mode number. So the numerical simulation can be performed in the cross section of the microcylinder as shown in Fig. 2, with the FDTD calculating window bounded by Γ_a, Γ_b, Γ_c, and Γ_d, where R, d, and d_1 are the radius, the thicknesses of the center layer and the upper cladding layer, respectively. The refractive index distribution in the z direction is $n(z)$ of $n_2/n_1/n_2/n_3$, where n_1 is the refractive index of the center layer and n_2 is that of the cladding layers and the substrate. The perfect matched layer absorbing boundary condition in circular cylindrical coordinates is used on Γ_a, Γ_c, and Γ_d [16], with the boundaries Γ_a, Γ_c, and Γ_d are placed 5, 5, and 4 μm away from the center layer's upper, lower, and lateral boundaries, respectively. The spatial steps Δz and Δr are set to be 10 and 20 nm, respectively, and the time step Δt is chosen to satisfy the Courant condition. At the inner boundary Γ_b at $r=4\Delta r$, the condition $\psi_m \propto r^m$ is used for the E_z and H_z field components based on the asymptotic behavior of the Bessel function [15]. In the simulation, an exciting source with a cosine impulse modulated by a Gaussian function $P(x_0,y_0,t)=\exp[-(t-t_0)^2/t_w^2]\cos(2\pi ft)$ is added to one component of the electromagnetic fields at a point (x_0,y_0) inside the microcylinder, where t_0 and t_w are the times of the pulse center and the pulse half width, respectively, and f is the center frequency of the pulse. The time variation of a selected field component at some points inside the microcylinder is recorded as a FDTD output, next the Padé approximation with Baker's algorithm [17] is used to transform the FDTD output from the time domain to the frequency domain, and then the mode frequencies and Q factors are calculated from the obtained intensity spectrum.

IV. NUMERICAL RESULTS

First, we consider a vertically symmetrical microcylinder with the $n(z)$ of $n_2/n_1=3.4/n_2$, $d=0.2$ μm, and $R=1$ μm. For the vertical fundamental mode, the electric field and magnetic field of TE WGMs are symmetrical and antisymmetric about $z=0$ plane in the symmetrical microcylinder, respectively, and TM WGMs are reversed. So symmetry sources about $z=0$ plane on electric field and magnetic field can be used to excite the TE and TM WGMs, respectively. The mode wavelengths and Q factors of the $TE_{7,1}$ (mode A) and $TM_{7,1}$ (mode B) WGMs are plotted versus n_2 in Fig. 3 as the open and solid squares and circles, respectively. The wavelengths of $TE_{7,1}$ and $TM_{7,1}$ WGMs have a crossover point at $n_2=2.3$, which indicates that mode coupling between the two WGMs does not exist in the symmetrical microcylinder. The Q factor of the $TE_{7,1}$ WGM gradually decreases

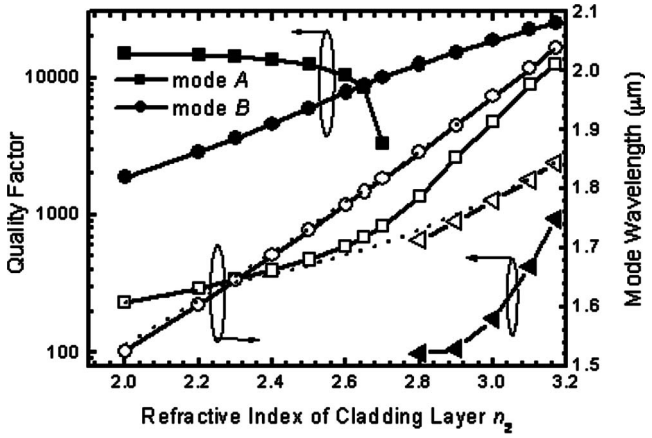

FIG. 3. Mode wavelengths (Q factors) of $TE_{7,1}$ (mode A) and $TM_{7,1}$ (mode B) WGMs versus n_2 are plotted as the open (solid) squares and circles, respectively, for the symmetrical microcylinder with the radius $R=1$ μm, $d=0.2$ μm, and the $n(z)$ of $n_2/n_1=3.4/n_2$. The dotted lines are mode wavelengths of $TE_{7,1}$ and $TM_{7,1}$ WGMs obtained from 2D eigenvalue equations under effective index approximation. The open and solid triangles are the mode wavelength and Q factor of $TE_{7,1}$ WGM after the anticrossing mode coupling.

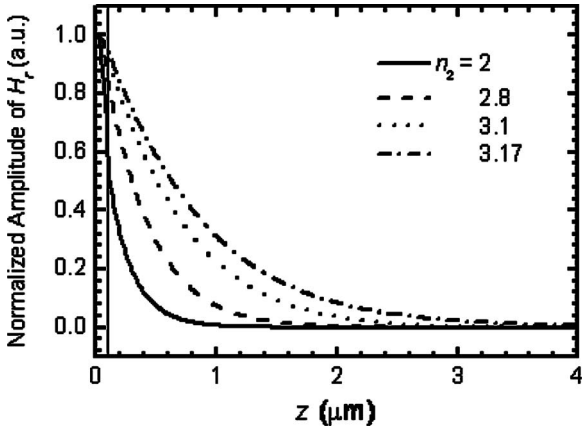

FIG. 4. Field distribution of $H_r(z)$ at $r=0.84$ μm for the $TM_{7,1}$ WGMs at $n_2=2$, 2.8, 3.1, and 3.17 in the symmetrical microcylinder of Fig. 3.

from 1.5×10^4 to 1.0×10^4 as n_2 increases from 2 to 2.6, and then rapidly decreases as $n_2>2.6$. As $n_2>2.8$, two peaks appear in the TE mode field spectra, which are correspondence to the anticrossing mode coupling between $TE_{7,1}$ and $HE_{7,1}$ modes. After the anticrossing mode coupling, $TE_{7,1}$ WGM becomes the vertical propagation $HE_{7,1}$ mode with a much smaller Q factor, which is not presented in Fig. 3 because the corresponding mode peak obtained from different time series of FDTD output is unstable. Furthermore, the $HE_{7,1}$ mode transfers to $TE_{7,1}$ WGM with the mode wavelength and Q factor marked as open and solid triangles in Fig. 3, respectively; the corresponding Q factor increases from 98 to 941 as n_2 increases from 2.8 to 3.17. The mode wavelengths of $TE_{7,1}$ and $TM_{7,1}$ WGMs obtained from the 2D eigenvalue equation [12] under the effective index approximation are also plotted as the dotted lines in Fig. 3, which agrees very well with the results of 3D FDTD simulation for $TM_{7,1}$, WGM. But the results of the eigenvalue equation for $TE_{7,1}$ WGM agree with the wavelength of mode A as $n_2<2.6$ and the wavelength of the mode marked by triangles as $n_2>2.8$, respectively. The Q factor of the $TM_{7,1}$ WGM increases from 1.9×10^3 to 2.5×10^4 as n_2 increases from 2 to 3.17, which is much larger than that of the $TE_{7,1}$ WGM as $n_2>2.7$. Because the horizontal radiation loss decreases with the increase of n_2 and the vertical radiation is absent, the Q factor of the $TM_{7,1}$ WGM can increase with the increase of n_2 from 2.0 to 3.17. Similarly in a photonic crystal slab, the forbidden coupling between the guided modes and the diffracted radiation field in air due to their symmetry mismatching can result in some guided modes above the light line with extremely long lifetimes [18].

Using a long optical pulse with a narrow bandwidth to excite only one mode, we can obtain the mode field distribution by the FDTD simulation. Figure 4 depicts the distribution of H_r (z) for $TM_{7,1}$ WGM at $r=0.84$ μm, where the vertical solid line is the upper boundary of the center layer. Because the field distribution is symmetrical about the $z=0$ plane, we only present the field distribution at $z>0$. With the increase of n_2, the field distribution becomes wide, but is still confined well as $n_2=2.0$, 2.8, 3.1, and 3.17.

For an asymmetric microcylinder with $d=0.2$ μm, $d_1=0.4$ μm, $R=1$ μm, and the $n(z)$ of $n_2/n_1=3.4/n_2/n_3=1$, we calculate and plot mode wavelengths and Q factors for the $TE_{7,1}$ and $TM_{7,1}$ WGMs versus n_2 in Fig. 5. The mode wavelengths of the $TE_{7,1}$ and $TM_{7,1}$ WGMs increase linearly with the increase of n_2, and the two modes have a weak anticrossing mode coupling at $n_2=2.31$, where they split with a minimum mode wavelength difference of 4.1 nm to prevent mode crossing. In the nonsymmetric microcylinder, the electromagnetic fields of $TE_{7,1}$ and $TM_{7,1}$ WGMs do not have the perfect symmetry characteristics relative to the $z=0$ plane, so they can have anticrossing mode coupling. Mode A is the $TE_{7,1}$ WGM with Q factor of 1.5×10^4 at $n_2=2.2$, and its Q factor suddenly drop to 6.9×10^3 due to the anticrossing mode coupling at $n_2=2.31$, and finally transfers

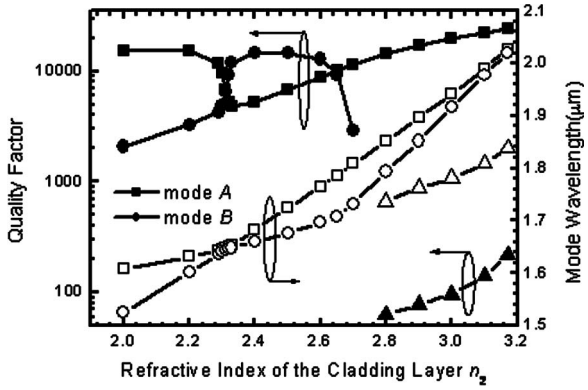

FIG. 5. Mode wavelengths and Q factors of the mode A (squares) and mode B (circles) versus n_2 for an asymmetric microcylinder with $d=0.2$ μm, $d_1=0.4$ μm, $R=1$ μm, and the $n(z)$ of $n_2/n_1=3.4/n_2/n_3=1$. The open and solid triangles are the mode wavelength and Q factor of $TE_{7,1}$ WGM after the anticrossing mode coupling.

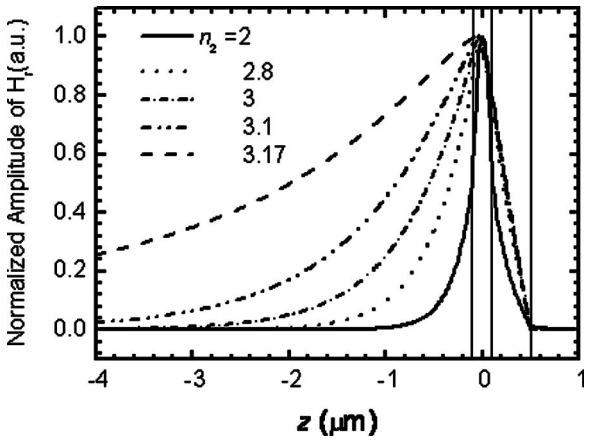

FIG. 6. Field distribution of $H_r(z)$ at $r=0.84$ μm for the mode A at $n_2=2.8$, 3, 3.1, and 3.17, and mode B at $n_2=2$ in the asymmetrical microcylinder of Fig. 5.

to $TM_{7,1}$ WGM when $n_2>2.33$ with the Q factor increases to 2.4×10^4 at $n_2=3.17$. Mode B is the $TM_{7,1}$ WGM with Q factor of 3.3×10^3 at $n_2=2.2$ and transfers to $TE_{7,1}$ WGM as $n_2>2.33$ with the Q factor equals 6.5×10^3 and 1.4×10^4 at $n_2=2.31$ and 2.5, respectively, but decreases rapidly when $n_2>2.6$ as in Fig. 3. Similarly, the $HE_{7,1}$ mode transfers to $TE_{7,1}$ WGM with the mode wavelength and Q factor marked as open and solid triangles as $n_2>2.8$ with the Q factor less than 200. Figure 6 shows the distribution of $H_r(z)$ at $r=0.84$ μm for mode A at $n_2=2.8$, 3, 3.1, and 3.17, and mode B at $n_2=2$ obtained by FDTD simulation under a single mode exciting source. Because of the large field tail in the low cladding layer, Γ_c is placed 10.0 μm under the center layer's low boundary when $n_2=3.17$. The field distribution becomes much wider than that in Fig. 4 as $n_2=3.17$, and the asymmetry of field distribution increases with the increase of n_2. However, the field profile is still confined well for mode A at $n_2=3.17$. For a strong asymmetric microcylinder as discussed in [19], the TM WGM cannot have a high Q factor as $n_2>2.8$ because the asymmetric slab waveguide cannot support TM guided mode.

Finally, we compare the mode wavelengths and Q factors obtained by the 3D FDTD simulation and the scattering-matrix method proposed in [11] for $TM_{m,1}$ WGMs in the symmetric microcylinder with the same structure parameters as Fig. 3 and $n_2=3.17$. As shown in Table I, the two methods yield almost the same mode wavelengths and Q factors as the azimuthal mode number $m=7$, 8, 9, and 10. The TM WGMs have Q factors larger than 2.5×10^4, which indicates that the vertical radiation loss is very small for the TM WGMs. In contrast, 3D FDTD simulation gives Q factor of

TABLE I. Mode wavelengths and Q factors obtained by 3D FDTD simulation and the scattering matrix for $TM_{m,1}$ WGMs in the symmetric microcylinder with $R=1$ μm, $d=0.2$ μm, $n_1=3.4$, and $n_2=3.17$.

	3D FDTD		Scattering matrix	
m	λ (μm)	Q	λ (μm)	Q
7	2.0398	2.52×10^4	2.0386	2.60×10^4
8	1.8281	1.23×10^5	1.8270	1.30×10^5
9	1.6586	6.54×10^5	1.6576	6.71×10^5
10	1.5195	3.50×10^6	1.5186	3.66×10^6

941, 878, 678, and 541 for $TE_{m,1}$ WGMs as $m=7$, 8, 9, and 10, respectively, due to the strong vertical radiation loss. Additionally, we calculate Q factors of the above modes in microcylinder with a 0.4 μm thickness center layer, the Q factors of TM WGMs are 3.73×10^4, 2.00×10^5, 1.12×10^6, and 6.39×10^6, respectively, and the Q factors of TE WGMs are 344, 277, 231, and 197, respectively. Accounting that the vertical waveguiding is mainly related to the refractive index difference and the difference between 3.4 and 3.17 is a medial value in GaAs and InP material systems, we expect that high Q factor TM WGMs are easy to realize in real semiconductor microcylinders.

V. CONCLUSION

We have demonstrated that high-Q TM WGMs can exist in semiconductor microcylinders with symmetry or weak asymmetry vertical waveguiding by 3D FDTD simulation. We observed the mode coupling between TE and TM WGMs in the microcylinders with asymmetry vertical waveguiding and the mode coupling between TE WGM and the vertical propagating HE mode, which induces a radiation loss and a low Q factor for TE WGMs. The mode wavelengths of TM WGMs are usually larger than the cutoff wavelengths of the radiated HE and EH modes with the same azimuthal and radial mode numbers, so the corresponding mode-coupling radiation loss is absent. Microlasers and single photon sources based on TM WGMs can be expected using semiconductor microcylinders with high current injection efficiency.

ACKNOWLEDGMENTS

This work was supported by the National Nature Science Foundation of China under Grant No. 60225011 and the Major State Basic Research Program under Grant No. 2006CB302804.

[1] K. J. Vahala, Nature (London) **424**, 839 (2003).
[2] J. M. Gérard and B. Gayral, J. Lightwave Technol. **17**, 2089 (1999).
[3] P. Michler, A. Kiraz, C. Becher, W. V. Scoenfeld, P. M. Petroff, L. Zhang, E. Hu, and A. Imamoğlu, Science **290**, 2282 (2000).
[4] M. Pelton, C. Santori, J. Vučković, B. Zhang, G. S. Solomon, J. Plant, and Y. Yamamoto, Phys. Rev. Lett. **89**, 233602 (2002).

[5] Y. Akahane, T. Asano, B.-S. Song, and S. Noda, Nature (London) **425**, 944 (2003).
[6] S. L. McCall, A. F. J. Levi, R. E. Slusher, S. J. Pearton, and R. A. Logan, Appl. Phys. Lett. **60**, 289 (1992).
[7] M. Fujita, R. Ushigome, and T. Baba, IEEE Photon. Technol. Lett. **13**, 403 (2001).
[8] M. Borselli, K. Srinivasan, P. E. Barclay, and O. Painter, Appl. Phys. Lett. **85**, 3693 (2004).
[9] M. Arzberger, G. Böhm, M.-C. Amann, and G. Abstreiter, Appl. Phys. Lett. **79**, 1766 (2001).
[10] N. C. Frateschi and A. F. J. Levi, Appl. Phys. Lett. **66**, 2932 (1995).
[11] X. S. Luo, Y. Z. Huang, W. H. Guo, Q. Chen, M. Q. Wang, and L. J. Yu, J. Opt. Soc. Am. B **23**, 1068 (2006).
[12] M. Hentschel and K. Richter, Phys. Rev. E **66**, 056207 (2002).
[13] K. S. Yee, IEEE Trans. Antennas Propag. **14**, 302 (1966).
[14] A. Taflove and S. C. Hagness, *Computational Electrodynamics: the Finite-Difference Time-Domain Method*, third ed. (Artech House, Boston/London, 2005).
[15] B.-J. Li and P.-L. Liu, IEEE J. Quantum Electron. **32**, 1583 (1996).
[16] T. G. Jurgens, *Proceedings of the 1995 IEEE MTT-s International Microwave Symposium*, Orlando, FL (IEEE, New York, 1995), p. 35.
[17] W. H. Guo, W. J. Li, and Y. Z. Huang, IEEE Microw. Wirel. Compon. Lett. **11**, 223 (2001).
[18] T. Ochiai and K. Sakoda, Phys. Rev. B **63**, 125107 (2001).
[19] X. S. Luo, Y Z. Huang, and Q. Chen, Opt. Lett. **31**, 1073 (2006) (The modes named as $HE_{7,2}$ and $HE_{6,2}$ in this article should be $TM_{7,1}$ and $TM_{6,1}$, respectively.)